ChemComm

Check for updates

Ion mobility mass spectrometry and molecular dynamics simulations unravel the conformational stability of zinc metallothionein-2 species†

Manuel David Peris-Díaz, [ID] *[ab] Alexey Barkhanskiy,[b] Ellen Liggett,[b] Perdita Barran [ID] *[b] and Artur Krężel [ID] *[a]

Ion mobility-mass spectrometry (IM-MS) unraveled different conformational stability in Zn_{4-7}-metallothionein-2. We introduced a new molecular dynamics simulation approach that permitted the exploration of all of the conformational space confirming the experimental data, and revealed that not only the Zn–S bonds but also the α–β domain interactions modulate protein unfolding.

Mammalian metallothioneins (MTs) constitute small ($\sim$6–7 kDa) cysteine-rich proteins with a biological role primarily in Zn^{2+} and Cu^+ metabolism.[1–3] At least a dozen MT isoforms (MT1–MT4) and multiple subisoforms have been found, which differ in their metal-binding properties, and tissue and cellular localization.[4,5] MTs have proved to be highly challenging objects to study using traditional biophysical techniques due to the lack of secondary structures and aromatic amino acids, and the spectroscopic silence of Zn^{2+}.[4] To date, only one X-ray structure has been solved for rat hepatic mixed Cd_5Zn_2MT2 species[6] The protein adopts a dumbbell shape with two metal-thiolate clusters named α- and β-domains containing a Cd_4Cys_{11} and $Cd_1Zn_2Cys_9$ cluster, respectively. Despite the capabilities of Cd^{2+} and Zn^{2+} to form an M_7MT2 (where M represents a metal ion), there is a divergence of behavior in the thermodynamic and kinetic properties between these two divalent metal ions, which is not without biological consequences.[7] The seven Cd^{2+} ions bind cooperatively in Cd_7MT in a domain fashion three to five orders of magnitude tighter than Zn^{2+}.[2] In contrast to cadmium, zinc MT2 presents three classes of affinities towards the seven Zn^{2+} ions. Four Zn^{2+} are bound with $K_d \sim 10^{-12}$ M, another two with $K_d \sim 10^{-10}$–10^{-11} M, while the seventh is weakly bound with K_d of $\sim 10^{-8}$ M.[8] As a consequence of this fact, MT2 exists as multiple $Zn_{4-7}MT2$

species under cellular conditions where the free Zn^{2+} concentration varies from 10^{-11} to 10^{-9} M.[9,10] The characterization of isolated MT fractions from several tissues and cell lines supported the role of $Zn_{4-7}MT2$ species as a zinc buffering system.[10–12] The heterogeneity of these species impedes their study by high-resolution structural techniques like cryo-EM, X-ray crystallography, or NMR. Ion mobility-mass spectrometry (IM-MS) has proven well-suited to interrogate heterogeneous protein systems and characterize their conformation and dynamics.[13–15] However, the resolution of the IM device may not be enough to separate closely related protein conformations. In some cases, gas-phase activation of protein ions *via* collisional activation, also referred to as Collision Induced Unfolding (CIU),[16] can be used to probe subtle structural differences between similar conformations and study protein ion stability and dynamics. Recently, high-resolution cyclic IM-MS based on traveling wave technology was introduced, allowing for tandem IM workflows.[17–19] Despite the structural information that can be derived from IM-MS experiments, it is unable to define protein structure at the atomic level. Recent efforts have focused on the integration of molecular dynamics (MD) with IM-MS, assigning gas-phase structures from *in silico* methods.[20–24] Unfortunately, usually only a few metastable states are explored since biological processes such as protein unfolding or conformational changes are on time scales far beyond those accessible by classical MD simulations. To access other conformational states, such as those sampled during CIU, most of the works have used a thermal unfolding approach. While some reports have shown that thermal unfolding can reproduce many general features observed during a CIU experiment,[20,24,25] a recent report has suggested a low reproducibility and lack of conformational sampling.[23]

In order to investigate the conformational properties of $Zn_{4-7}MT2$ species and shed more light on how these species resemble at the microscopic level, IM-MS, CIU, and MD simulations were integrated. The nESI mass spectra of apoMT2 in the presence of tris(2-carboxyethyl)phosphine hydrochloride (TCEP) (termed as "red") present a charge state distribution (CSD) spanning only three charge states $3 \leq z \leq 5$, with $apoMT2^{5+}_{red}$ and

[a] Department of Chemical Biology, Faculty of Biotechnology, University of Wrocław, F. Joliot-Curie 14a, 50-383 Wrocław, Poland.
  E-mail: manuel.perisdiaz@uwr.edu.pl, artur.krezel@uwr.edu.pl
[b] Michael Barber Centre for Collaborative Mass Spectrometry, Manchester Institute of Biotechnology, 131 Princess Street, Manchester, M1 7DN, UK.
  E-mail: perdita.barran@manchester.ac.uk
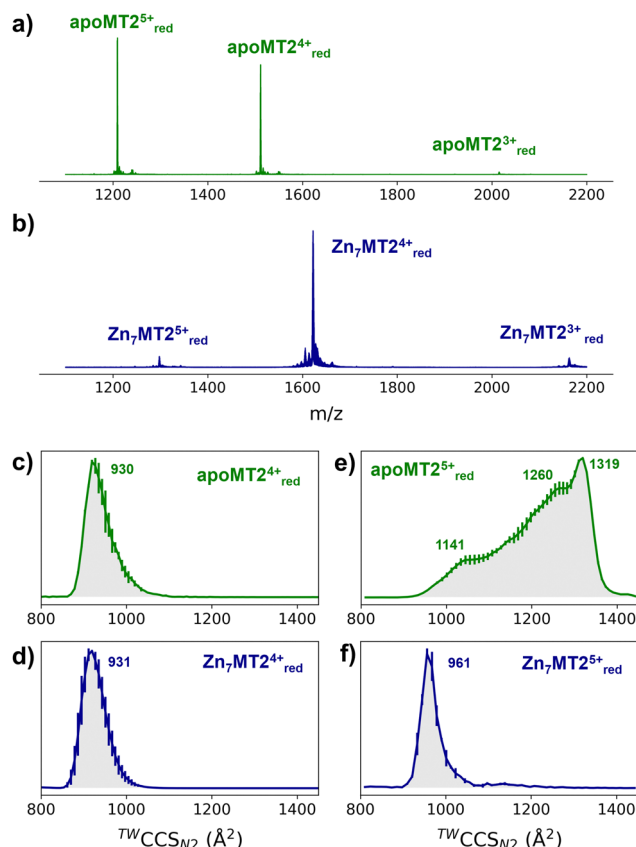
Fig. 1 Native mass spectra of apoMT2 and Zn_7MT2 (a and b) and travelling wave (TW) ion mobility (IM)-derived collision cross sections (CCS) (c–f) of quadrupole-selected apoMT2 and Zn_7MT2 5+ and 4+ ions. The proteins (10 μM) were sprayed in 50 mM ammonium acetate (pH 6.8) in the presence and absence of 1 mM neutralized TCEP (pH 7.4). Red refers to the reduced state of the ions, as TCEP was on-line employed during the measurement. The CCS values were calculated from three replicates, and the error bars are plotted along the CCS axis.

$apoMT2^{4+}_{red}$ the most dominant (Fig. 1a). Reconstituted Zn_7MT2 protein exhibits a CSD shift toward lower charge state with the $Zn_7MT2^{4+}_{red}$ ions predominant (Fig. 1b), suggesting that solution-phase conformational changes alter the solvent accessible surface area (SASA). The $apoMT2^{4+}_{red}$ and $Zn_7MT2^{4+}_{red}$ ions displayed a similar collision cross section (CCS) (Fig. 1c and d), hereby not representing the SASA changes.

The CCS for $apoMT2^{5+}_{red}$ presents a broad CCS distribution, and upon Zn^{2+} binding, a single and compact $Zn_6MT2^{5+}_{red}$ and $Zn_7MT2^{5+}_{red}$ conformer is observed (Fig. S1, ESI†). IM-MS revealed that 5+ ions undergo a conformational change capturing the CSD shift observed in the mass-to-charge spectrum (Fig. 1e and f). Partially Zn^{2+}-loaded MT2 species were obtained *via* titration in the presence of TCEP, and native IM-MS under different collisional activation (CA) conditions were recorded (Fig. S2, ESI†). Metal-coupled folding effects can be observed upon Zn^{2+} binding to $apoMT2^{5+red}$: prior to CA, $Zn_{4-7}MT2^{5+}_{red}$ ions populate a CCS $\sim$ 1000 Å^2 *cf.* $\sim$ 1300 Å^2 for $apoMT2^{5+}_{red}$ (Fig. S2, ESI†). As the collision energy is increased, the CCS shifts to $\sim$1150 Å^2 in all of the $Zn_{4-7}MT2$ complexes. Similar results were obtained under 50 or 200 mM ammonium acetate (Fig. S3, ESI†). Unpredictably,

fitting the native mass spectra to simulated isotopic distributions revealed the partial retention of protons within the Zn^{2+} clusters. Lacking a reducing agent during spraying generates signals shifted to lower m/z (Fig. S2, ESI†). Mass spectra simulations estimated the formation of 7–8 disulfides for all $Zn_{4-6}MT2^{5+}_{ox}$ and 2 disulfides for $Zn_7MT2^{5+}_{ox}$ (Table S1, ESI†). As a consequence, while some portion of the ions unfold to $\sim$1150 Å^2, as in the case of reduced complexes, most of the ions are trapped at $\sim$1000 Å^2. To compare the gas-phase stabilities of $Zn_{4-7}MT2^{5+}$ ions, the CCS along the collisional energy assayed were fitted to estimate the CIU_{50} values to indicate the energy required to activate 50% of the ions to the next conformation.[16] A similar $CIU_{50} \sim$ 90 eV was calculated for $Zn_4MT2^{5+}_{red}$ and $Zn_5MT2^{5+}_{red}$ ions (Fig. S4, ESI†). A gradual increase to $CIU_{50} \sim$ 110 eV was then determined for $Zn_6MT2^{5+}_{red}$ and $Zn_7MT2^{5+}_{red}$. Our previous study provided the location of Zn^{2+} in all $Zn_{4-7}MT2$ species.[26] In Zn_4MT2, two Zn^{2+} are bound in each α- and β-domain forming Zn_2Cys_6 clusters. The fifth Zn^{2+} binds to the α-domain forming an $αZn_3Cys_9$ cluster. The sixth Zn^{2+} saturates the α-domain forming an $αZn_4Cys_{11}$ cluster, and the seventh Zn^{2+} forms the $βZn_3Cys_9$ cluster. CIU did not detect structural changes between Zn_2Cys_6 and Zn_3Cys_9 clusters but determined elevated structural stability upon the formation of the Zn_4Cys_{11} cluster. Taken together, our results elucidated a plausible structural explanation for why the seventh Zn^{2+} ion binds with a K_d of $\sim 10^{-8}$ M to MT2 and provided a link between structural and Zn^{2+} buffering properties.[8]

To get further structural insights into the existing conformational families, we employed multistage IM-MS using a cyclic IM-MS instrument. Upon activation of isolated compact conformer α, we observe an unfolding profile that leads largely to a conformation γ, through a β intermediate conformation and a minor extended δ conformation (Fig. 2a–c). The great potential of tandem IM is that it allows not only the examination of the unfolding mechanisms but also the evaluation of the thermodynamic and kinetic stability of the unfolded conformations.[18] Isolation of the conformer γ (Fig. 2d) and subsequent CIU activation leads to an unfolding profile with no new features (Fig. 2e). We do not evidence a sign of interconversion to a compact conformation (Fig. 2f). These results suggest that there exists a relatively high transition energy barrier between these states, and propose a plausible irreversible unfolding mechanism that yields a thermodynamically stable conformation that can be of relevant interest under cellular stress conditions.
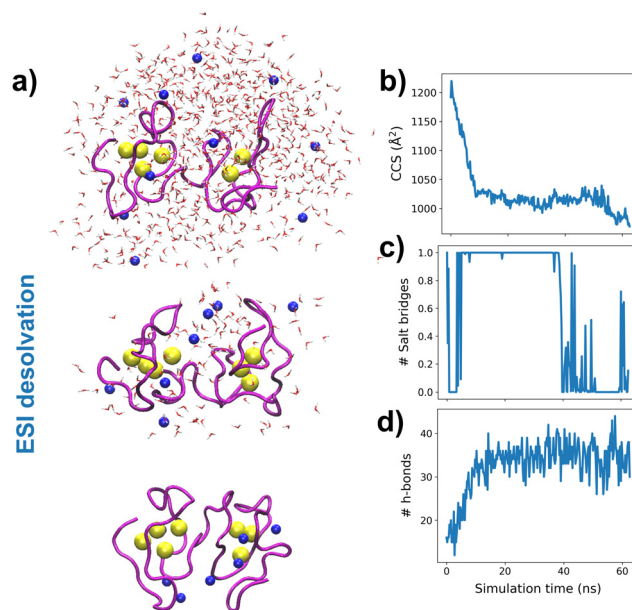
To understand the experimental results from a microscopic point of view, we then performed gas-phase MD simulations (Fig. 3a). We first focused on examining how the $Zn_{4-7}MT2$ protein complexes are transferred from the solution into the gas-phase (Fig. S5–S10, ESI†). Proteins were placed in aqueous nanodroplets with an excess of charge to 16+ using Na^+ as a charge carrier rather than H^+. As the simulation evolves, the solvent gradually evaporates, and Na^+ ions are ejected until a charge decrease to 5+. Droplet shrinkage is accompanied by a decrease in the CCS from $\sim$1200 to 1000 Å^2 until the structure collapses to a more compact conformation with CCS $\sim$ 950 Å^2 without altering the Zn–S bonds (Fig. S5–S10 and Fig. 3b, ESI†). In this process, salt bridges do not appear to modulate the transition from solution to gas-phase,[27] but the collapse of the structure is highlighted by an increased number of h-bonds from $\sim$20 to $\sim$40 (Fig. 3c and d). Such results

Fig. 2 Multistage cyclic IM-MS experiments. Arrival time distribution (ATD) recorded for the mass-selected $Zn_7MT2^{5+}_{red}$ ions (1298 m/z) under non-activating conditions (a) and activated on injection to the trap prior to IM selection (d). The IMS-CA-IMS and CA-IMS-CA-IMS approach in which the conformer α (b) and conformer γ (e) were isolated and reinjected from the pre-store into the array at increasing activation energies, respectively. Unfolding profiles for the IMS-CA-IMS (c) and CA-IMS-CA-IMS approach (f).

Fig. 3 Molecular dynamics simulations. Snapshots of the desolvation process at different simulation times for an aqueous nanodroplet containing Zn_7MT2 and Na^+ as a charge carrier (a) and analysis of CCS (b), salt-bridges (c) and h-bonds (d) as a function of desolvation time. Yellow and blue spheres represent Zn^{2+} and Na^+, respectively, and the solvent molecule oxygen atoms are shown in red. The protein backbone is shown in magenta.

are in excellent agreement with our experimental native IM-MS data (max error < 5%) and shed light on the gas-phase desolvation and protein structure at the atomic level. We then attempted to simulate the CIU of electrosprayed protein complexes. First, a thermal unfolding protocol was performed on representative structures obtained from gas-phase MD desolvation simulations (Fig. 4a and b). All of the protein ions have narrower ΔCCS than the recorded experimental CIU data (Fig. 4a): $apoMT2^{5+}_{red}$ has a ΔCCS of 400 Å^2 vs. ΔCCS 300 Å^2 for simulations, and $Zn_{4-7}MT2^{5+}_{red}$ has a ΔCCS of 200–250 Å^2 vs. ΔCCS 70–150 Å^2 for simulated proteins. SA identified multiple conformations for $apoMT2^{5+}$, a compact conformation of ∼1000 Å^2, and a semi-extended one of ∼1200 Å^2, although the extended one with CCS ∼1300 Å^2 was not sampled (Fig. 4b). Similarly, the compact and semi-extended conformers were present in $\alpha Zn_2\beta Zn_2MT2^{5+}$ and $\alpha Zn_3\beta Zn_1MT2^{5+}$, and once again, the extended conformation was not detected. As the Zn^{2+} loading increases, the conformational heterogeneity measured as the CCS (ΔCCS) decreases, indicating that Zn^{2+} promotes protein folding. Consequently, simulations for Zn_5MT2^{5+} and higher Zn^{2+}-loaded states only sampled the compact conformations (Fig. 4b). Extending the simulation times from 10 to 100 ns did not influence the conformational sampling. Therefore, thermal unfolding failed to overcome the energetic

restraints imposed by the Zn–S bonds and was not able to sample extended conformations obtained upon collisional activation. As the radius of gyration (R_g) correlated well with the CCS values, we used an enhanced sampling algorithm named steered MD (SMD) simulations to accelerate the transitions between different states by using R_g as a collective variable (CV). The force-CCS profiles obtained by SMD simulations clearly distinguished the compact α and extended conformation β and reproduce well their ΔCCS (Fig. 4c and Fig. S11–S17, ESI†). Comparable CCS distributions were obtained when using the end-to-end N-C terminus distance as a CV (Fig. S18–S24, ESI†). We observed that protein unfolding proceeds via destabilizing the interdomain α–β interactions (Fig. 3a). To examine their mechanostability properties, average unfolding forces were calculated from 25 SMD replicates (Fig. S25a and b, ESI†). SMD cannot be quantitatively compared to CIU experiments as the physical principles underlying these approaches are different. However, we found similarities as the low linear correlation between the mean unfolding force and the number of Zn^{2+} bound to MT2 (Fig. S25b, ESI†). To estimate more accurate protein unfolding, we performed well-tempered metadynamics simulations (Fig. S25c, ESI†). Similar conclusions were obtained as with SMD. Examining the protein conformations, we observed a linear relationship between h-bonds and Zn–S bonds (Fig. S25d, ESI†). Interestingly, neither mean unfolding forces nor estimated free energies were correlated with h-bonds or Zn–S bonds (Fig. S25e, ESI†). These results indicate that protein unfolding is not only controlled by metal–S interactions or h-bonds but also other energetic forces contribute to this process. To date, no single report has characterized the structure and protein conformations for physiologically relevant zinc MT2 species. Here IM-MS aided by MD

Fig. 4 Collision cross section (CCS) profiles for the quadrupole-selected apoMT2^{5+}red and Zn$_{4-7}$MT2^{5+}red species under different collisional activation energies (a). Gaussian kernel density estimate (KDE) for 300 K, 500 K and 800 K slices from thermal unfolding simulations (b). Gaussian KDE for steered MD simulations with 10, 25 and 50 kcal mol^{-1} nm^{-2} force constants (c). Representative snapshots for the conformations from each protein species labeled as in the Gaussian KDE (d). Yellow and blue spheres represent Zn^{2+} and Na$^+$, respectively, and the protein backbone is shown in grey.

simulations present a comprehensive structural characterization of these protein complexes. Collectively, our study provides a plausible link between structural and Zn^{2+} buffering properties and sheds light on the mode of functioning of these small yet critical cellular proteins. In addition, as thermal unfolding has been shown not only here but also in other studies that may lack conformational sampling, we report an alternative MD framework to simulate CIU experiments.

Conflicts of interest

There are no conflicts to declare.

Notes and references

1 A. Krężel and W. Maret, *Int. J. Mol. Sci.*, 2017, **18**, 1237.

2 M. J. Stillman, *Coord. Chem. Rev.*, 1995, **144**, 461–511.

3 M. R. Mehlenbacher, *et al.*, *Chem. Sci.*, 2022, **13**, 5289–5304.

4 A. Krężel and W. Maret, *Chem. Rev.*, 2021, **121**, 14594–14648.

5 E. Artells, O. Palacios, M. Capdevila and S. Atrian, *Metallomics*, 2013, **5**, 1397–1410.

6 W. Braun, *et al.*, *Proc. Natl. Acad. Sci. U. S. A.*, 1992, **89**, 10124–10128.

7 M. D. Peris-Díaz, *et al.*, *Anal. Chem.*, 2020, **92**, 12950–12958.

8 A. Krężel and W. Maret, *J. Am. Chem. Soc.*, 2007, **129**, 10911–10921.

9 A. Krężel and W. Maret, *J. Biol. Inorg. Chem.*, 2006, **11**, 1049–1062.

10 Y. Yang, W. Maret and B. L. Vallee, *Proc. Natl. Acad. Sci. U. S. A.*, 2001, **98**, 5556–5559.

11 A. Krężel and W. Maret, *Mol. Med.*, 2007, **13**, 371–375.

12 A. Krężel and W. Maret, *Biochem. J.*, 2007, **402**, 551–558.

13 S. M. Bargeen, *et al.*, *Nat. Commun.*, 2022, **13**, 4377.

14 S. C. Wang, *et al.*, *J. Am. Chem. Soc.*, 2010, **132**, 15468–15470.

15 I. Michaelevski, M. Eisenstein and M. Sharon, *Anal. Chem.*, 2010, **82**, 9484–9491.

16 S. M. Dixit, D. A. Polasky and B. T. Ruotolo, *Curr. Opin. Chem. Biol.*, 2018, **42**, 93–100.

17 K. Giles, *et al.*, *Anal. Chem.*, 2019, **91**, 8564–8573.

18 C. Eldrid, *et al.*, *J. Am. Soc. Mass Spectrom.*, 2021, **32**, 1545–1552.

19 E. Deslignière, *et al.*, *J. Am. Soc. Mass Spectrom.*, 2021, **32**, 2505–2512.

20 R. Beveridge, *et al.*, *J. Am. Chem. Soc.*, 2019, **141**, 4908–4918.

21 E. G. Marklund, *et al.*, *Structure*, 2015, **23**, 791–799.

22 A. D. Rolland, L. S. Biberic and J. S. Prell, *J. Am. Soc. Mass Spectrom.*, 2022, **33**, 369–381.

23 C. Eldrid, *et al.*, *Anal. Chem.*, 2022, **94**, 16113–16121.

24 S. Nash and R. W. Vachet, *J. Am. Chem. Soc.*, 2022, **144**, 22128–22139.

25 J. Bellamy-Carter, *et al.*, *Analysis Sensing*, 2021, **1**, 63–69.

26 M. D. Peris-Díaz, *et al.*, *J. Am. Chem. Soc.*, 2021, **143**, 16486–16501.

27 L. Konermann, E. Aliyari and J. H. Lee, *J. Phys. Chem. B*, 2021, **125**, 3803–3814.